

NUMERICAL SIMULATION OF AN ELASTOMER IN A METALFORMING PROCESS

Mariela Luege, Bibiana Luccioni*

Instituto de Estructuras
Universidad Nacional de Tucumán,* CONICET.
Av. Roca 1800. S.M. de Tucumán, Argentina. Tel./Fax: 0381-4364087.
email: bluccioni@herrera.unt.edu.ar

Key Words: Tube hydroforming, Elastomer Materials, Internal Variables, Finite Element Method, Industrial Application.

Abstract. *The use of elastomers as pressure media in the tube hydroforming technology has received increasing interest especially for the production of lightweight and complicated forming components, because of uniform pressure application that confers more ductility to the pieces being conformed. In order to understand how the different parameters, such as the hardness of the components and the intensity of the applied loads on the blankhold, interact in the forming process, it is essential to define the elastomer behavior accurately. This is the focus of the present work.*

The behavior of the elastomer is characterized by high deformability, nonlinear stress-strain response, damping, rate independent hysteresis and quasiincompressibility. Within the framework of continuum thermodynamics of irreversible processes with internal variables and large strains, the formulation of a phenomenological constitutive law is presented. A visco-hyperelastic model with associated plasticity in finite strains, the algorithm for its numerical integration, and its implementation in an explicit dynamic finite element code are described. Application examples related to a product of cosmetic industry are analysed, together with the influence of different parameters in the forming process.

1 INTRODUCTION

The hydroforming technology is widely used today in the production of low cost and lightweight components for the automotive, aerospace and household industries compared with traditional forming processes. Among the hydroforming processes, the tube hydroforming technology presents several advantages, such as weight reduction, improved part strength and stiffness, and lower tooling cost.¹ In its simplest scheme, this technology consists of a combined loading of compression forces at the tube ends as well as an hydrostatic internal pressure applied by a viscous medium. These loads expand the tube and lead to the alignment of the tube wall with the outside surface of the die cavity. Conventionally tube hydroforming processes use a fluid as pressure medium. However, elastomers also can be used in their place. In this case, the advantage is an improved sealing that reduces leakage and allows easier handling in prototype production of a small number of parts.²

This paper is focused on the study of poliurethane elastomers as viscous pressure medium in tube hydroforming processes. For the high pressures that are involved, however, the elastomer exhibits a large range of plasticity in addition to viscoelastic behaviour. Starting from a one dimensional rheological model as motivation, where both behaviors are taken into account, a generalization of the constitutive model to large strain, using the multiplicative decomposition of the deformation gradient and continuum thermodynamics of irreversible processes with internal variables for the definition of the state and evolution laws is presented. Then, the algorithm for the numerical integration of the constitutive equations for the implementation into an explicit finite element code is sketched and finally FE predictions for the control of some process conditions of an industrial application in cosmetic industry are described.

2 RHEOLOGICAL MODEL

The rheological model shown in Figure 1 represents a one-dimensional model in small strain exhibiting elastoplastic and viscoelastic behaviour. ϵ_{EQ}^e , ϵ_{EQ}^p and ϵ_{NEQ}^e , ϵ_{NEQ}^i denote elastic and inelastic deformation of the equilibrated (rate-independent) and nonequilibrated (rate-dependent) components, respectively, with σ_{EQ} and σ_{NEQ} the respective stresses.

The model consists of an elastoplastic element with hardening defined by the internal kinematic variables (ϵ_{EQ}^e , ϵ_{EQ}^p , α) and the conjugate forces (σ_{EQ} , R), coupled in parallel to a viscoelastic element defined in terms of (ϵ_{NEQ}^e , ϵ_{NEQ}^i) and the nonequilibrated stress or over-stress σ_{NEQ} . Kinematic and equilibrium conditions relating ϵ_{EQ}^e , ϵ_{EQ}^p , ϵ_{NEQ}^e , ϵ_{NEQ}^i to ϵ , and σ_{EQ} , σ_{NEQ} to σ , together with the state laws and the evolution laws for ϵ_{EQ}^p , α , ϵ_{NEQ}^i complete the constitutive model. For the model shown in Figure 1, considering the relaxation process under controlled deformation, the equilibrium state is identified when the stress reaches asymptotically a constant value, with the nonequilibrated stress σ_{NEQ} dissipated in time according to the defined evolution laws.

Different viscoelastic and viscoplastic models can be developed systematically combining elementary rheological models starting from basic assumptions on equilibrium, kinematic and constitutive laws of the elementary components.³

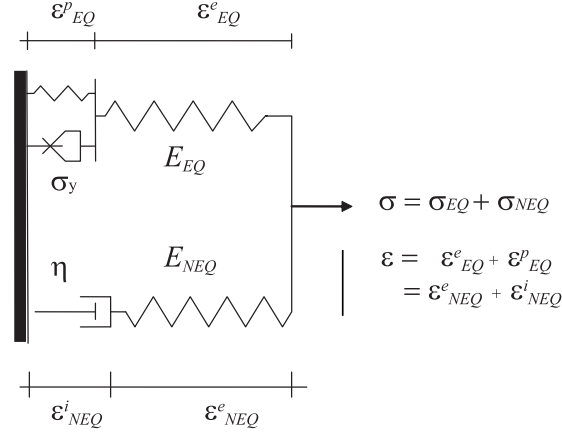


Figure 1: A 1D rheological model with viscoelastoplastic behaviour.

3 BASIC ASSUMPTIONS OF THE CONSTITUTIVE MODEL

Let φ denote the deformation of the reference configuration Ω to the current one Ω_φ , $\mathbf{F} = \nabla\varphi$ the deformation gradient, $\mathbf{C} = \mathbf{F}^T\mathbf{F}$ and $\mathbf{b} = \mathbf{F}\mathbf{F}^T$ the right and left Cauchy-Green deformation tensors, respectively. Using as motivation the rheological model described in Section 2, a multiplicative decomposition of \mathbf{F} into inelastic parts, \mathbf{F}_{EQ}^p and \mathbf{F}_{NEQ}^i , and elastic parts, \mathbf{F}_{EQ}^e and \mathbf{F}_{NEQ}^e , for the equilibrated and nonequilibrated parts, is assumed. That is,

$$\mathbf{F} = \mathbf{F}_{EQ}^e \mathbf{F}_{EQ}^p = \mathbf{F}_{NEQ}^e \mathbf{F}_{NEQ}^i. \quad (1)$$

The decomposition (1) corresponds to the assumption of a plastic unstretched intermediate configuration⁴ and of a viscous unstretched intermediate configuration⁵ which are only locally defined. Due to the modular structure of the model, an additive split of the total free energy function Ψ is assumed

$$\Psi = \Psi_{EQ} + \Psi_{NEQ}, \quad (2)$$

where Ψ_{EQ} and Ψ_{NEQ} are the contributions associated with the equilibrated (rate-independent) and nonequilibrated (rate-dependent) part of the model, respectively. For the isotropic response under consideration, Ψ_{EQ} and Ψ_{NEQ} depend only on the left Cauchy-Green strain tensor \mathbf{b}_{EQ}^e and \mathbf{b}_{NEQ}^e defined in terms of \mathbf{F}_{EQ}^e and \mathbf{F}_{NEQ}^e , respectively. The component Ψ_{EQ} is also assumed to depend on the hardening parameter α to account for energy storage due to hardening effects.⁶

For the formulation of state and evolution laws, the equation of the internal dissipation is required to hold for all admissible processes. Such a dissipation for isothermal processes is written as⁷

$$\mathcal{D}_{int} = \mathbf{S} : \frac{1}{2} \dot{\mathbf{C}} - \dot{\Psi} \geq 0, \quad (3)$$

with \mathbf{S} the second Piola-Kirchhoff stress tensor related to the Cauchy stress $\boldsymbol{\sigma}$ as follows

$$\mathbf{S} = J \mathbf{F}^{-1} \boldsymbol{\sigma} \mathbf{F}^{-T},$$

and $J = \det \mathbf{F}$. Replacing (2) into (3) and standard arguments give the following state laws

$$\boldsymbol{\sigma} = 2 J^{-1} \mathbf{b}_{EQ}^e \frac{\partial \Psi_{EQ}}{\partial \mathbf{b}_{EQ}^e} + 2 J^{-1} \mathbf{b}_{NEQ}^e \frac{\partial \Psi_{NEQ}}{\partial \mathbf{b}_{NEQ}^e} = \boldsymbol{\sigma}_{EQ} + \boldsymbol{\sigma}_{NEQ}, \quad R := \frac{\partial \Psi_{EQ}}{\partial \alpha}, \quad (4)$$

with R the thermodynamic force conjugate of α and

$$\boldsymbol{\sigma}_{EQ} := 2 J^{-1} \mathbf{b}_{EQ}^e \frac{\partial \Psi_{EQ}}{\partial \mathbf{b}_{EQ}^e}, \quad \boldsymbol{\sigma}_{NEQ} := 2 J^{-1} \mathbf{b}_{NEQ}^e \frac{\partial \Psi_{NEQ}}{\partial \mathbf{b}_{NEQ}^e}. \quad (5)$$

By accounting of (4), and after some rearrangements, the dissipation inequality reduces to

$$\mathcal{D}_{int} = -\text{dev} \boldsymbol{\tau}_{EQ} : \frac{1}{2} \mathcal{L}_{\boldsymbol{\chi}}\mathbf{b}_{EQ}^e^{-1} - \text{dev} \boldsymbol{\tau}_{NEQ} : \frac{1}{2} \mathcal{L}_{\boldsymbol{\chi}}\mathbf{b}_{NEQ}^e^{-1} - R \dot{\alpha} \geq 0, \quad (6)$$

where the Kirchhoff stress tensors and the Lie derivative of the material tensor field \mathbf{a} defined as follows, have been introduced

$$\boldsymbol{\tau}_{EQ} := J \boldsymbol{\sigma}_{EQ}, \quad \boldsymbol{\tau}_{NEQ} := J \boldsymbol{\sigma}_{NEQ}, \quad \mathcal{L}_{\boldsymbol{\chi}}[\mathbf{a}] := \boldsymbol{\chi}^* \left[\frac{d}{dt} \left(\boldsymbol{\chi}^{*-1}[\mathbf{a}] \right) \right], \quad (7)$$

with $\boldsymbol{\chi}^{*-1}[\mathbf{a}] := \mathbf{F}^{-1} \mathbf{a} \mathbf{F}^{-T}$ the *pull-back* operation of the spatial field \mathbf{a} to the reference configuration, and $\boldsymbol{\chi}^*[\mathbf{a}] = \mathbf{F} \mathbf{a} \mathbf{F}^T$ the *push-forward* of \mathbf{a} .⁷

The evolution laws are then obtained by defining $\mathcal{L}_{\boldsymbol{\chi}}\mathbf{b}_{EQ}^e^{-1}$, $\mathcal{L}_{\boldsymbol{\chi}}\mathbf{b}_{NEQ}^e^{-1}$ and $\dot{\alpha}$ as functions of $\boldsymbol{\tau}_{EQ}$, $\boldsymbol{\tau}_{NEQ}$ and R , upon the condition that (6) is met.

4 FORMULATION OF THE CONSTITUTIVE MODEL

Within the general framework set in the previous Section, the model proposed in this paper is specified by defining the free energy Ψ and the evolution laws for $\mathcal{L}_{\boldsymbol{\chi}}\mathbf{b}_{EQ}^e^{-1}$, $\mathcal{L}_{\boldsymbol{\chi}}\mathbf{b}_{NEQ}^e^{-1}$ and $\dot{\alpha}$.

4.1 Free energy function and state laws

The components Ψ_{EQ} and Ψ_{NEQ} of the free energy Ψ are assumed to be a sum of an isochoric (constant volume) and volumetric contribution, as follows

$$\Psi = \Psi_{EQ}^{iso}(\bar{\mathbf{b}}_{EQ}^e, \alpha) + \Psi_{NEQ}^{iso}(\bar{\mathbf{b}}_{NEQ}^e) + \Psi_{EQ}^v(J_{EQ}) + \Psi_{NEQ}^v(J_{NEQ}), \quad (8)$$

with $\bar{\mathbf{b}}_{EQ}^e$ and $\bar{\mathbf{b}}_{NEQ}^e$ the distortional part of \mathbf{b}_{EQ}^e and \mathbf{b}_{NEQ}^e , respectively, and $J_{EQ} = \det \mathbf{F}_{EQ}^e$ and $J_{NEQ} = \det \mathbf{F}_{NEQ}^e$.

For the isochoric parts of Ψ , Ψ_{EQ}^{iso} and Ψ_{NEQ}^{iso} , an hyperelastic Ogden energy for incompressible materials is adopted. This energy function is more conveniently expressed as a function

of modified principal strains $(\bar{\lambda}_{EQ A}^e)_{A=1,2,3}$, and $(\bar{\lambda}_{NEQ A}^e)_{A=1,2,3}$, principal values of $\bar{\mathbf{F}}_{EQ}^e$ and $\bar{\mathbf{F}}_{NEQ}^e$, respectively, that is,

$$\begin{aligned}\Psi_{EQ}^{iso}(\bar{\mathbf{b}}_{EQ}^e, \alpha) &= \sum_{p=1}^N \frac{\mu_p}{\alpha_p} \left(\sum_{A=1}^3 (\bar{\lambda}_{EQ A}^e)^{\alpha_p} - 3 \right) + \frac{H}{2} \alpha^2 \\ \Psi_{NEQ}^{iso}(\bar{\mathbf{b}}_{NEQ}^e, \beta) &= \sum_{r=1}^N \frac{\mu_r^{vp}}{\alpha_r^{vp}} \left(\sum_{A=1}^3 (\bar{\lambda}_{NEQ A}^e)^{\alpha_r^{vp}} - 3 \right),\end{aligned}\tag{9}$$

with (K, α_p, μ_p, H) and $(K^{vp}, \alpha_r^{vp}, \mu_r^{vp})$ material constants for the equilibrated and nonequibrated part, respectively.

For the volumetric parts, Ψ_{EQ}^v and Ψ_{NEQ}^v , a quadratic law vanishing when the respective Jacobian equals the unity, is assumed. That is,

$$\Psi_{EQ}^v(J_{EQ}) = \frac{1}{2} K (J_{EQ} - 1)^2, \quad \Psi_{NEQ}^v(J_{NEQ}) = \frac{1}{2} K^{vp} (J_{NEQ} - 1)^2.\tag{10}$$

By accounting for (9) and (10), from (4)₁ and (8), the following equation is obtained

$$\boldsymbol{\sigma} = \text{dev} \boldsymbol{\sigma}_{EQ} + \text{dev} \boldsymbol{\sigma}_{NEQ} + p \mathbf{I},\tag{11}$$

with

$$\begin{aligned}\text{dev} \boldsymbol{\sigma}_{EQ} &= 2 J^{-1} \mathbf{b}_{EQ}^e \frac{\partial \Psi_{EQ}^{iso}}{\partial \bar{\mathbf{b}}_{EQ}^e}(\bar{\mathbf{b}}_{EQ}^e) : \frac{\partial \bar{\mathbf{b}}_{EQ}^e}{\partial \mathbf{b}_{EQ}^e}, \\ \text{dev} \boldsymbol{\sigma}_{NEQ} &= 2 J^{-1} \mathbf{b}_{NEQ}^e \frac{\partial \Psi_{NEQ}^{iso}}{\partial \bar{\mathbf{b}}_{NEQ}^e}(\bar{\mathbf{b}}_{NEQ}^e) : \frac{\partial \bar{\mathbf{b}}_{NEQ}^e}{\partial \mathbf{b}_{NEQ}^e},\end{aligned}$$

and

$$p := K \frac{J_{EQ}}{J} (J_{EQ} - 1) + K^{vp} \frac{J_{NEQ}}{J} (J_{NEQ} - 1),$$

whereas the hardening law reads as

$$R = H \alpha.\tag{12}$$

4.2 Evolution laws for the internal variables

For the definition of the evolution laws, the dissipative mechanisms associated with the plastic and viscous behaviour of the material are assumed to be uncoupled. By accounting of (6), this assumption leads to the following two inequalities that must be independently satisfied

$$-\text{dev} \boldsymbol{\tau}_{EQ} : \frac{1}{2} \mathcal{L}_{\boldsymbol{\chi}}\mathbf{b}_{EQ}^e^{-1} - R \dot{\alpha} \geq 0, \quad -\text{dev} \boldsymbol{\tau}_{NEQ} : \frac{1}{2} \mathcal{L}_{\boldsymbol{\chi}}\mathbf{b}_{NEQ}^e^{-1} \geq 0.\tag{13}$$

For the treatment of the plastic part, the Von Mises yield function defined in terms of the equilibrated part of the Kirchhoff stress for the principle of objectivity, is introduced

$$\mathcal{F}(\boldsymbol{\tau}_{EQ}, R) = \|\text{dev}\boldsymbol{\tau}_{EQ}\| - \sqrt{\frac{2}{3}}(\sigma_y + R), \quad (14)$$

with σ_y the yield stress, and the following evolution equation for the plastic flow,⁸ is defined

$$-\frac{1}{2}(\mathcal{L}_{\boldsymbol{\chi}}[\mathbf{b}_{EQ}^e]) (\mathbf{b}_{EQ}^e)^{-1} = \dot{\lambda} \frac{\partial \mathcal{F}}{\partial \boldsymbol{\tau}_{EQ}} = \dot{\lambda} \frac{\text{dev}\boldsymbol{\tau}_{EQ}}{\|\text{dev}\boldsymbol{\tau}_{EQ}\|}, \quad \dot{\alpha} = -\dot{\lambda} \frac{\partial \mathcal{F}}{\partial R} = \sqrt{\frac{2}{3}} \dot{\lambda} \quad (15)$$

together with the Kuhn–Tucker conditions

$$\dot{\lambda} \geq 0; \quad \mathcal{F} \leq 0; \quad \dot{\lambda} \mathcal{F} = 0. \quad (16)$$

On the other hand, the following equation is considered for the dissipation associated with the viscous part,⁹

$$-\frac{1}{2}(\mathcal{L}_{\boldsymbol{\chi}}[\mathbf{b}_{NEQ}^e]) (\mathbf{b}_{NEQ}^e)^{-1} = \frac{1}{\eta} \text{dev}\boldsymbol{\tau}_{NEQ}. \quad (17)$$

This equation corresponds to a quadratic viscous dissipation potential $\Phi = \frac{1}{\eta} \|\text{dev}\boldsymbol{\tau}_{NEQ}\|^2$. It is then an easy matter to check that (15), (16) and (17) meet (13)₁ and (13)₂, respectively, ensuring the thermodynamical consistency of the constitutive model.

5 NUMERICAL INTEGRATION

Since the viscoelastic and plastic evolution laws are decoupled, the integration of the constitutive equations of the model under consideration is carried out independently using algorithms proposed in literature for multiplicative finite strain elastoplasticity⁸ and finite viscoelasticity.⁹ Both the algorithms are derived via an operator split of the local evolution problems into an elastic predictor followed by the plastic and viscoelastic corrector. The elastic predictor is computed exactly, whereas the inelastic corrections are realized separately by means of exponential mapping algorithms in order to satisfy exactly the viscous and plastic incompressibility. Due to the material isotropy, the algorithmic equations can be expressed in principal directions.

6 NUMERICAL EXAMPLE

The finite element modeling of a ridge on an aluminum tube by the tube hydroforming process with polyurethane elastomer as viscous pressure media is discussed in this section.

Figure 2 shows a scheme of the test device. This consists of a die cavity which gives the ridge's shape with radius $R_d = 8.635 \text{ mm}$, the aluminum cylinder with inner radius $R_c = 8.235 \text{ mm}$ and thickness $t = 0.38997 \text{ mm}$, the forming media represented by an elastomer with radius $R_e = 8.235 \text{ mm}$, the punch and the blankholder.

The elastomer behaviour is defined by the constitutive model described in the previous section and has been implemented in the explicit finite element code STAMPACK[®].¹⁰ For the

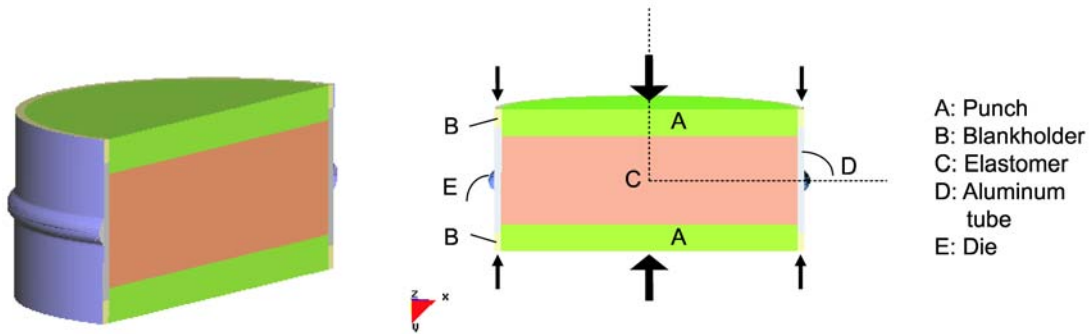


Figure 2: Stamping tools for the forming process of a ridge with the tube hydroforming technique.

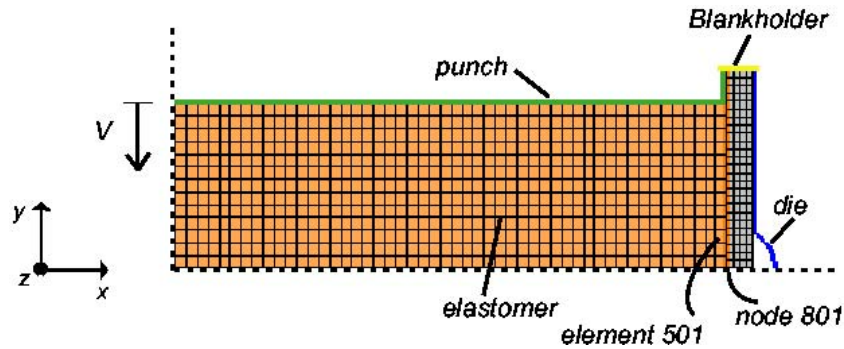


Figure 3: Finite Element model for the stamping of the ridge.

friction between the elastomer and the aluminum tube, a modified version of Coulomb law with velocity dependent coefficient friction and taking into account different lubrication regimes has been assumed.¹¹ The value of the static and kinetic friction coefficient are set equal to $\mu_s = 2$ and $\mu_k = 0.01$, respectively, with normal and tangential penalty coefficient $K_N = K_T = 0.1$, while the aluminum–die interface is modelled as pure viscous for the interposition of a lubricant layer.

In the forming process, the two punches are moved at constant velocity against the elastomer that pushes the aluminum tube into the die cavity. In order to agevolute the forming process the blankholder can apply a linearly increasing force or be constrained to have the same displacement as the punches. The process will terminate when the ridge is completely formed and the punches are released to return to their original configuration.

The finite element model of the process is displayed in Figure 3, where axisymmetric 4–node bilinear isoparametric elements are used. Due to the symmetry of the problem only one quarter of the specimen will be analysed. The analysis purpose is the evaluation of the influence on the forming process of: (i) two elastomers of different hardness and (ii), the use of different blankhold load conditions.

In the first example, two types of elastomer, type A and type B, are considered. They correspond to hardness A65 and A80, respectively. Elastomer type B has higher hardness than

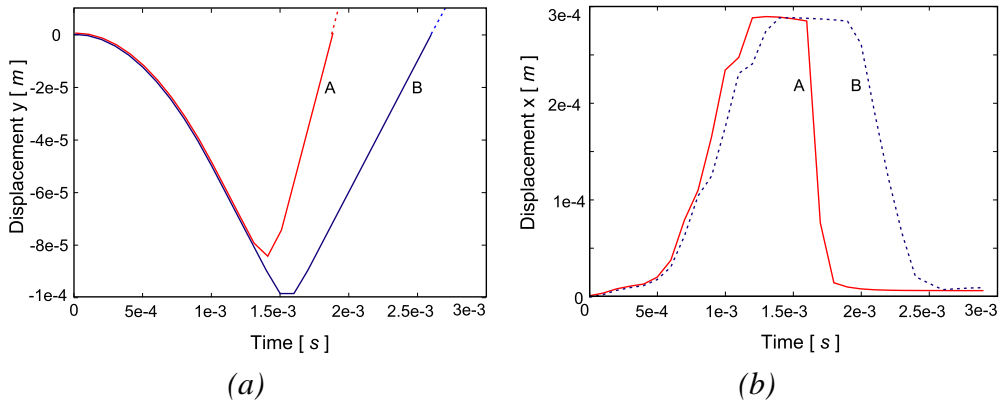


Figure 4: Time history for (a) the displacement of the punch and (b) the displacement in direction x of the elastomer node 801 for the elastomers type A and type B.

elastomer type A. The maximum value of the blankhold load P is assumed to be equal to $10 N$. The material properties of the two elastomers are given in Table 1. The aluminum tube is modelled as an elastic–perfectly plastic material with a Prandtl–Reuss evolution law, and the following material constants: $E = 0.6e + 11 N/m^2$, $\nu = 0.33$, $\sigma_y = 1.19393e + 8 N/m^2$,

Type	α_1	$\mu_1 [N/m^2]$	$K [N/m^2]$	$\tau [s]$	v_{rel}	$\sigma_y [N/m^2]$	$H [N/m^2]$
A	3.09132	1049088.554	1.0e10	720.0	0.54041	1.2e6	0
B	3.09132	29204819.3	1.0e10	10800	0.498	1.2e7	0

Table 1: Material constants used for the elastomer. (α_1, μ_1) Ogden’s parameters; K bulk modulus; τ retardation time; $v_{rel} = \mu_1/\mu_{v1}$ ratio of the hyperelastic constants for the nonviscous and viscous part; σ_y yield stress; H hardening modulus. Stiffness μ_1 and retardation time τ of the elastomer type B are higher than that of the elastomer type A.

Figure 4(a) displays the time evolution of the punch displacement during the whole forming process for the two elastomers. The minimum value in these curves corresponds to the condition when the aluminum tube takes the shape of the die. This value is attained at $t_A = 1.4e - 3 s$ for the elastomer type A and at $t_B = 1.5e - 3 s$ for the elastomer type B. Figure 4(b), on the other hand, depicts the time evolution of the displacement along x of the node 801 of the elastomer. The shape of this curve gives indication of the evolution of the forming process with the ridge formation corresponding to the plateau in the curve. It may be noted that, once the punch is released and returned to its original configuration, the elastomer seems to recover more or less its original shape. Moreover, comparing the results of the two forming processes, it can be observed that for the elastomer type B the process duration ($\Delta t_B = 2.6e - 3 s$) is longer than that for the elastomer type A ($\Delta t_A = 1.9e - 3 s$), representing an important information on the number of pieces that can be performed.

Figure 5 shows a map of the value of the maximum principal deformation for both elas-

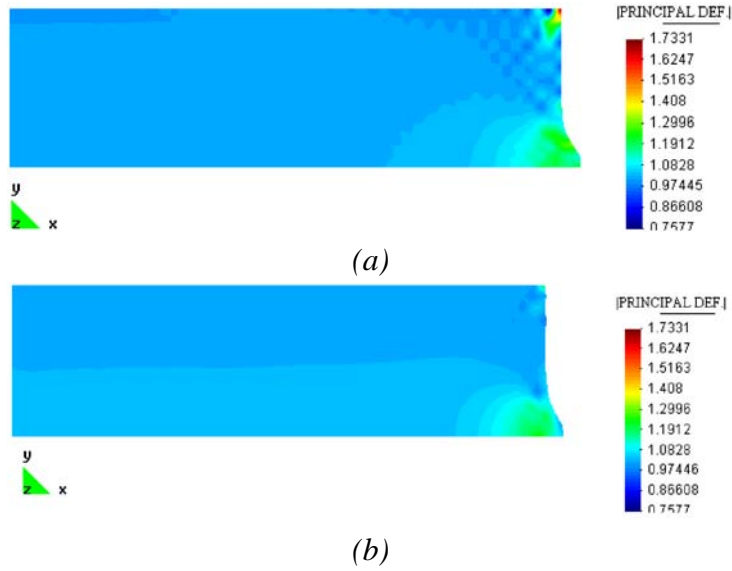


Figure 5: Map of the maximum principal deformation on the deformed configuration for (a) the elastomer type A at $t_A = 1.4e - 3 s$ and (b) the elastomer type B at $t_B = 1.5e - 3 s$.

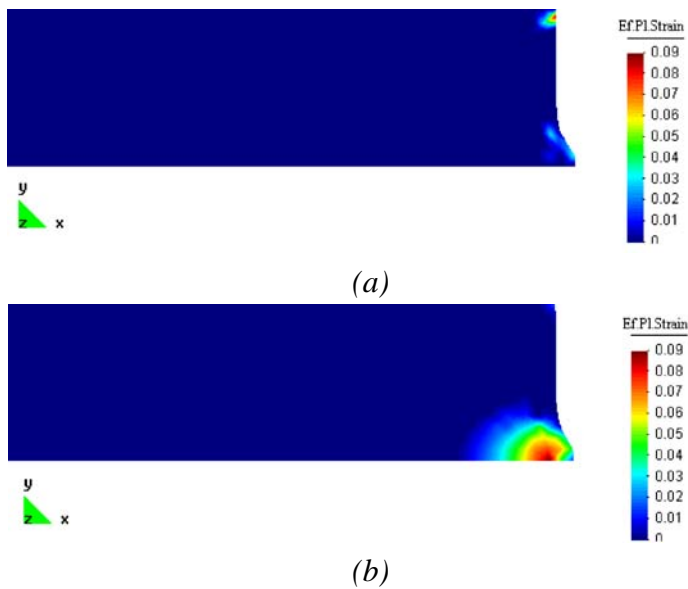


Figure 6: Map of the equivalent plastic deformation on the deformed configuration for (a) the elastomer type A at $t_A = 1.4e - 3 s$ and (b) the elastomer type B at $t_B = 1.5e - 3 s$.

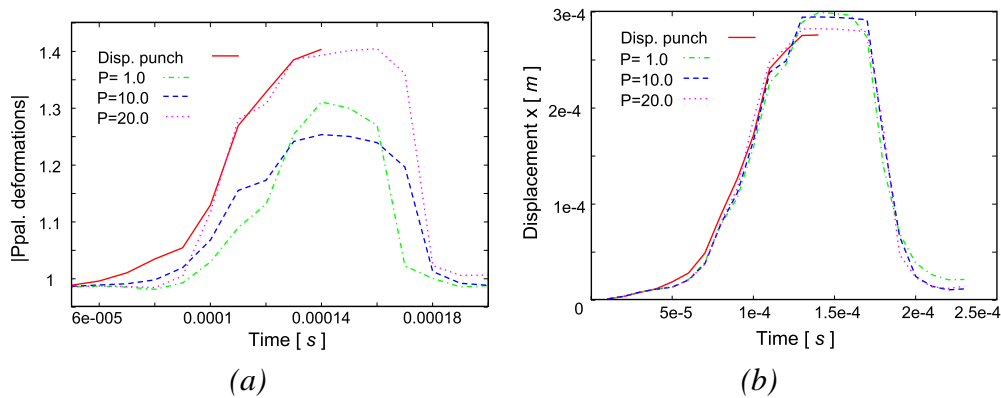


Figure 7: Results for the elastomer type A. Time history of (a) the maximum principal deformation in the element 501 for different blankholder conditions, and (b) the displacement in direction x of the node 801 for different blankholder conditions.

tomers, type A and type B, at $t_A = 1.4e - 3$ s and $t_B = 1.5e - 3$ s, respectively. High gradient deformations in the elastomer are observed in the region corresponding to the ridge (right bottom), and in the corner between the punch and the aluminum cylinder (right top). In the case of the elastomer type A, the principal deformation results higher near the punch which could lead the elastomer to flux over the punch if the distance punch–cylinder is not small enough. With regard to the plastic behaviour of the elastomers, Figure 6 depicts the map of the equivalent plastic deformation. It can be observed that, for both elastomers, the maximum equivalent plastic deformation is about 9% but differently distributed. Elastomer A has plastic deformations concentrated at the right top corner whereas in the elastomer type B the plastic deformations are concentrated at the right bottom near the ridge.

In order to evaluate the influence of different blankhold load conditions on the forming process, the elastomer type A is considered as viscous pressure media and the cases with the blankhold load $P = 1, 10, 20$ N and the case with the blankhold constrained to displace as the punch are examined. The latter condition is hereafter referred to as PBH.

Figure 7(a) shows the time evolution of the principal deformation modulus in the element 501 in correspondence of the die cavity. One can note that only for the case $P = 10$ N the maximum value of the deformation is below 1.25, meeting therefore a common elastomer manufacture recommendation to have the elastomer deformation below 25%.

Figure 7(b), on the other hand, depicts the time evolution of the displacement in direction x of the node 801 of the elastomer and gives indication on the forming process evolution, noticing in this case that there are not appreciable differences among the different blankhold cases considered.

Figures 8 and 9 display the equivalent plastic deformation map of an amplified elastomer–aluminium zone at $t_A = 1.4e - 3$ s. It can be noted that for the PBH condition, the equivalent plastic deformations in the elastomer appear both at the right top and bottom corner with value equal to 0.4218 in the alluminium near the ridge, whereas the presence of plastic deformations

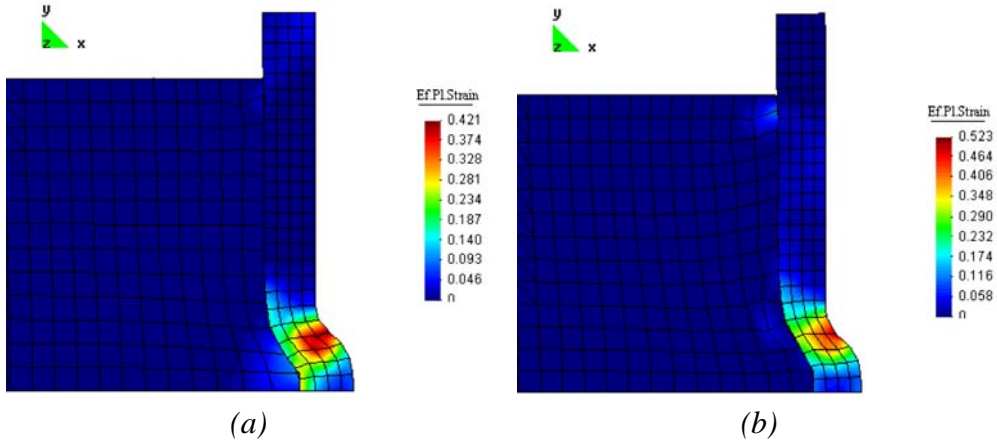


Figure 8: Contact zone between the elastomer type A and aluminum at $t_A = 1.4e - 3 s$ with superimposed map of the equivalent plastic deformation for: (a) the PBH condition and (a) $P = 1 N$.

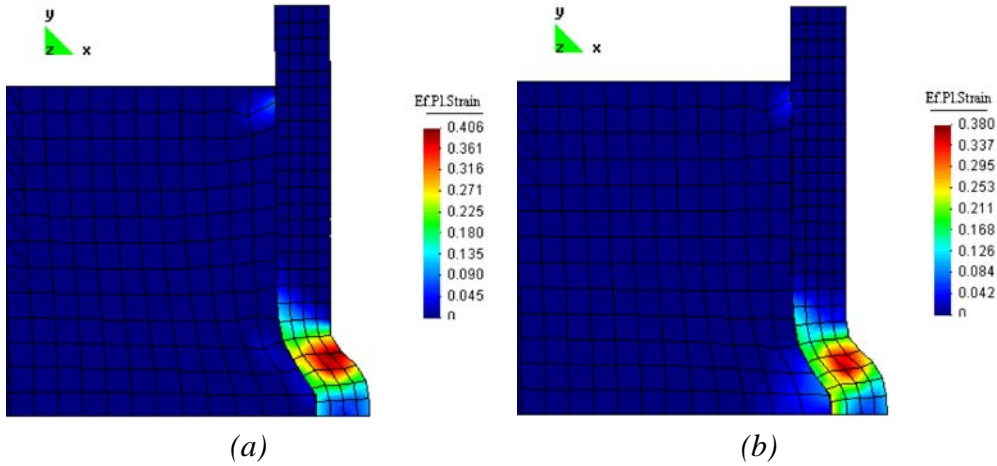


Figure 9: Contact zone between the elastomer type A and aluminum at $t_A = 1.4e - 3 s$ with superimposed map of the equivalent plastic deformation for: (a) $P = 10 N$ and (a) $P = 20 N$.

at the top of the cylinder near the blankholder could mean possible incipient buckling. When the blankholder load is $P = 1\text{ N}$, the equivalent plastic deformations in the elastomer appear mostly concentrated at the right top corner together, with an increase of the equivalent plastic deformation in the aluminum equal to 0.523. Increasing the load to $P = 10\text{ N}$ reduces the plastic deformations in the elastomer at the right top corner and in coincidence with the ridge (right bottom), and reduces the plastic deformation in the aluminum to 0.4065. Finally, by increasing the load to $P = 20\text{ N}$ the behaviour approaches to the PBH condition, with plastic deformations in the elastomer concentrated near the ridge.

7 CONCLUSIONS

Compared to conventional stamping processes, the tube hydroforming technology using elastomers as forming media is relatively new. As a result, there is still a relevant lack of knowledge on the influence of some operating parameters on the effectiveness of the whole process.

In order to show the capability of the finite element method as predictive and verifying tool, a constitutive model that accounts for the plastic and viscous dissipative mechanisms in the elastomer is developed within the framework of continuum thermodynamics with internal variables. Numerical simulations are carried out to analyse the influence of parameters such as the hardness of the elastomer and several blankhold conditions on the manufacturing of a ridge on an aluminum tube. The use of softer elastomers results in a reduction of the process duration influencing therefore the number of pieces that can be manufactured. This effect could be described because of the interplay between the Ogden's material parameters describing the hyperelastic response and the retardation time associated with the viscous behaviour. Also, the different blank hold conditions seem not having any appreciable influence on the process duration but rather on the inelastic deformations of the elastomer and of the aluminum tube.

The examples developed show, therefore, that further to an accurate modelling of the elastomer behaviour and of the contact conditions, the finite element model is able to give effective and useful indications about the forming process under consideration to the analyst and designer.

ACKNOWLEDGEMENTS

The authors gratefully acknowledge the financial support of the CONICET, Argentina, and Oscar Frutos from METALFORM[®] for providing them the data from the industrial application.

REFERENCES

- [1] Lang L.H., Wang Z.R., Kang D.C., Yuan S.J., Zhang S.H., Danckert J., and Nielsen K.B. Hydroforming highlights: sheet hydroforming and tube hydroforming. *J. of Materials Processing Technology*, **151**, 165–177 (2004).
- [2] Ahmetoglu M., Hua J., Kulukuru S., and Altan T. Hydroforming of sheet metal using a viscous pressure medium. *J. of Materials Processing Technology*, **146**, 97–107 (2004).
- [3] Haupt P. *Continuum Mechanics and Theory of Materials*. Springer Verlag, (2002).

- [4] Lee E.H. Elastic-plastic deformation at finite strains. *J. of Applied Mechanics*, **36**, 1–6 (1969).
- [5] Sidoroff F. Un modèle viscoélastique non linéaire avec configuration intermédiaire. *J. de Mécanique*, **13**, 679–713 (1974).
- [6] Besson J., Cailletaud G., Chaboche J.L., and Forest S. *Mécanique Non Linéaire des Matériaux*. Hermes Science Publications, (2001).
- [7] Simo J.C. Numerical analysis and simulation of plasticity. In Ciarlet P.G. and Lions J.L., editors, *Handbook of Numerical Analysis*, volume VI, pages 183–499. Elsevier Science, (1998).
- [8] Simo J.C. Algorithms for static and dynamic multiplicative plasticity that preserve the classical return mapping schemes of the infinitesimal theory. *Comput. Methods Appl. Mech. Engrg.*, **99**, 61–112 (1992).
- [9] Reese S. and Govindjee S. A theory of finite viscoelasticity and numerical aspects. *Int. J. Solids Structures*, **35**, 3455–3482 (1998).
- [10] STAMPACK[®]. Simulation software for multi-stage metal forming operations. Quantech. Barcelona, Spain.
- [11] Luege M. and Luccioni B. Finite strain model for elastomer-aluminum contact interface in forming processes. In *Proceedings of the Eighth International Conference on Computational Plasticity*. Barcelona, Spain, (2005).